

# Two new mononuclear zinc(II) and cadmium(II) coordination polymers based on 4-(3-pyridyl)-2H-1,2,3-triazole: Syntheses, structures, theoretical and fluorescent properties

Rong Zhao<sup>a</sup>, Yan-Jun Li<sup>a,\*</sup>, Yun-Feng Chen<sup>b</sup>, Ye Cong<sup>a</sup>, Jiang Zhang<sup>a</sup>, Zhi-Jun Dong<sup>a</sup>, Guan-Ming Yuan<sup>a</sup>, Zheng-Wei Cui<sup>a</sup>, Xuan-Ke Li<sup>a,c</sup>

<sup>a</sup> Hubei Province Key Laboratory of Coal Conversion and New Carbon Materials, School of Chemistry and Chemical Engineering, Wuhan University of Science and Technology, Wuhan 430081, People's Republic of China

<sup>b</sup> School of Chemistry and Environment Engineering, Wuhan Institute of Technology, Wuhan 430073, People's Republic of China

<sup>c</sup> State Key Laboratory of Refractories and Metallurgy, Wuhan University of Science and Technology, Wuhan 430081, People's Republic of China

## ARTICLE INFO

### Article history:

Received 11 December 2018

Accepted 19 March 2019

Available online 27 March 2019

### Keywords:

Coordination polymers

d<sup>10</sup> metal

Crystal structures

TD-DFT

Fluorescent properties

## ABSTRACT

Two new d<sup>10</sup> metal coordination polymers (CPs), [Zn(L)NO<sub>3</sub>]<sub>n</sub> (**1**) and [Cd(L)I<sub>2</sub>]<sub>n</sub> (**2**) (L = 4-(3-pyridyl)-2H-1,2,3-triazole), have been designed and synthesized from Zn<sup>II</sup>/Cd<sup>II</sup> ions and the rigid L ligand. The CPs **1** and **2** have been structurally characterized by single-crystal X-ray diffraction analyses, elemental analysis, IR spectroscopy, powder X-ray diffraction (PXRD) and thermal gravimetric analyses (TGA). CP **1** exhibits a *hcb* (3,3)-connected 2D network with the point symbol (6<sup>3</sup>) and further forms a supramolecular 3D structure via hydrogen bonds. CP **2** reveals a 1D straight chain constructed by units of [Cd(1)N<sub>2</sub>L<sub>4</sub>] and hydrogen bonding leads to the formation of supramolecular 3D system. In addition, time-dependent density functional theory calculations with B3LYP functional were performed on L, CPs **1** and **2** to rationalize their experimental absorption spectra. The luminescence properties of L, CPs **1** and **2** in solid-state and different solvents have been also investigated.

© 2019 Elsevier Ltd. All rights reserved.

## 1. Introduction

Coordination polymers (CPs), an emerging type of crystalline organic–inorganic hybrid materials made by linking inorganic and organic units. In the last three decades, CPs have attracted much research attention [1,2], and have shown promise in a wide range of applications from gas adsorption and storage [3], heterogeneous catalysis [4], photoluminescence [5] and chemical sensing [6], light harvesting [7,8], drug delivery and biological labeling [9,10]. The potential applications of CPs and their topological configurations are inseparable. At present, more and more CPs with topological structures have been reported, such as chain, ladder, square, hexagonal, diamond and cubic [11–14]. Through the construction of crystals with different topological structures, the assembly rules for the development of new crystalline materials may be found. The luminescent CPs have provoked increasing concern for researchers owing to their extensive applications including photocatalysis [15], photoluminescence [16–19] and electroluminescence [20]. The luminescence properties of these

complexes are closely related to the structural and electronic characteristics of their ligands [21,22]. The temperature of luminescent CPs as well as the surrounding medium, such as the solvent, counterions and neighboring complexes, also play an important role in their luminescence [23,24]. Various possible electron transitions of lowest excited singlet state to ground state have been observed while the luminescent CPs are excited, including  $\pi-\pi^*$  and  $n-\pi^*$  transitions from intraligand,  $d\sigma^*-p\sigma$  transitions from metal-to-ligand (MLCT) and  $d\sigma^*-\pi^*$  transitions from metal-metal-to-ligand (MMLCT) [25,26].

Recently, N-donor linkers have been widely adopted for the assembly of variable coordination networks. The 1,2,3-triazole is nitrogen rich heterocycle and could exhibit abundant coordination modes [27,28]. Moreover, nitrogen-containing heterocycles are easy to form hydrogen bonds, which is beneficial to the self-assembly of supramolecular structures, and multidentate 1,2,3-triazole based ligands forms various functional materials with tuning of the substituents on the triazole ring. For the introduction of nitrogenous pyridine groups enhances the coordination ability, facilitates the expansion of coordination networks, and promotes the ligand-centered  $\pi-\pi^*$  transition [29,30], we have added pyridine groups to 1,2,3-triazole and incorporate this conjugated

\* Corresponding author.

E-mail address: [yanwatercn@wust.edu.cn](mailto:yanwatercn@wust.edu.cn) (Y.-J. Li).

organic moiety into CPs. On the other hand, the complexes of  $d^{10}$  metal have attracted much attention owing to their diverse structures and photoluminescent behaviors [31–33]. In this work, we employ transition metal ions  $Cd^{2+}$ ,  $Zn^{2+}$  and the first prepared aromatic organic ligand 4-(3-Pyridyl)-2H-1,2,3-triazole (denoted as **L**) to assemble two new coordination complexes  $[Zn(L)NO_3]_n$  (**1**) and  $[Cd(L)I_2]_n$  (**2**). Moreover, the absorption properties, time-dependent density functional theory (TD-DFT) calculations and their fluorescence properties have also been investigated.

## 2. Experimental

### 2.1. Materials and physical measurements

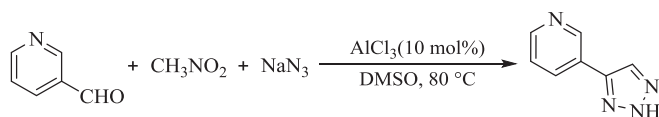
All chemicals and solvents were commercially available and used without further purification. Elemental analyses for C, H, and N were performed on an Elementar Vario EL elemental analyzer. FT-IR spectra were recorded from 4000 to 400  $cm^{-1}$  by a Bruker VERTEX 70 instrument with KBr pellets. Powder X-ray diffraction patterns (PXRD) were performed on a Philips Pert MPD Pro diffractometer using Cu K $\alpha$  radiation. Thermogravimetric analyses were carried out by a NETZSCH STA 449F3 thermal analyzer (30–800  $^{\circ}C$  range) at a heating rate of 10 K/min. The fluorescence spectra were measured on a F-7000 FL spectrophotometer instrument. UV–Vis absorption spectra were measured on a Shimadzu UV-2550 spectrophotometer in the  $BaSO_4$  plate. Mass spectra were recorded on Thermo DSQ II GC/MS mass spectrometer.

### 2.2. Preparations of ligand **L**

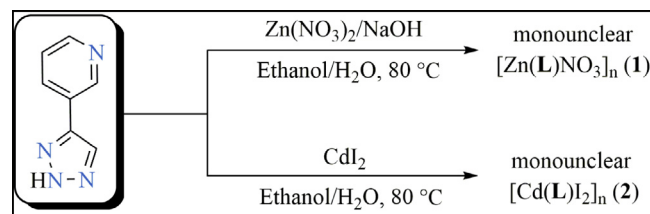
The ligand **L** has not been reported in the literature and has been synthesized through an efficient and convenient  $AlCl_3$ -catalyzed three-component condensation reaction of aromatic aldehydes, nitroalkanes and sodium azide [34]. The mixture of 3-Pyridinecarboxaldehyde (10.711 g, 0.10 mol), nitromethane (9.156 g, 0.15 mol),  $NaN_3$  (7.805 g, 0.12 mol), and  $AlCl_3$  (1.333 g, 0.01 mol), were stirred in DMSO (300 mL) at 80  $^{\circ}C$  under air for 8 h (Scheme 1). And then the solution was extracted with ethyl acetate ( $3 \times 300$  mL). The combined organic layers were washed with saturated sodium chloride solution ( $3 \times 300$  mL) and dried over anhydrous sodium sulphate, then the solvent was evaporated in vacuo to obtain a crude product. Finally, a yellowish solid of **L** was obtained by column chromatography.  $^1H$  NMR (600 MHz, DMSO- $d_6$ ),  $\delta$  9.05 (d,  $J = 2.1$  Hz, 1H), 8.53 (d,  $J = 4.8$  Hz, 1H), 8.45 (s, 1H), 8.20 (d,  $J = 7.9$  Hz, 1H), 7.46 (d,  $J = 7.9, 4.8$  Hz, 1H). IR (KBr pellets,  $cm^{-1}$ ):  $\nu(N-H)$  3147 w;  $\nu(C=N)$  1560 s;  $\nu(C=C)$  1432(s). MS  $m/z$ : 146.11 [ $M^+$ ] (calcd: 146.15).

### 2.3. Preparations of $[Zn(L)NO_3]_n$ (**1**)

A solution of  $Zn(NO_3)_2 \cdot 6H_2O$  (0.041 g, 0.136 mmol) in 0.5 mL  $H_2O$  was added to a solution of **L** (0.020 g, 0.136 mmol) in 2 mL ethanol. The mixture was sealed in a 20 mL glass bottle and heated at 80  $^{\circ}C$  for 3 days and cooled to room temperature naturally. Colorless rodlike crystals of **1** was obtained by filtration (Scheme 2). Yield: 0.022 g, 32%. Anal. Calc. (%) for  $C_7H_5N_5O_3Zn$ : C, 30.85; H, 1.85; N, 25.69. Found: C, 30.99; H, 1.97; N, 25.57. IR (KBr pellets,



Scheme 1. Synthesis of 4-(3-Pyridyl)-2H-1,2,3-triazole (**L**).



Scheme 2. Construction of CPs **1** and **2** with **L**.

$cm^{-1}$ ):  $\nu(N-H)$  3135 w;  $\nu(C=N)$  1617 m;  $\nu(C=C)$  1490 s;  $\nu(N-O)$  1380 w.

### 2.4. Preparations of $[Cd(L)I_2]_n$ (**2**)

A solution of  $CdI_2$  (0.050 g, 0.136 mmol) in 0.5 mL  $H_2O$  was added to a solution of **L** (0.020 g, 0.136 mmol) in 2 mL ethanol. The mixture was sealed in a 20 mL glass bottle and heated at 80  $^{\circ}C$  for 3 days and cooled to room temperature naturally. A colorless mixture was formed and filtered. The filtrate was evaporated at room temperature and colorless rodlike crystals of **2** were obtained after several days (Scheme 2). Yield: 0.042 g, 45%. Anal. Calcd (%) for  $C_{14}H_{12}N_8CdI_2$  for: C, 25.53; H, 1.84; N, 17.01. Found: C, 25.43; H, 1.90; N, 17.00. IR (KBr pellets,  $cm^{-1}$ ):  $\nu(N-H)$  3127 w;  $\nu(C=N)$  1610 m;  $\nu(C=C)$  1430 s.

### 2.5. Crystal structure determination

The single-crystal X-ray data of CPs **1** and **2** were collected with Mo K $\alpha$  radiation ( $\lambda = 0.071073$  nm) on a Bruker APEX II Smart CCD diffractometer at 293 (2) K. All the structures were solved by direct methods using the SHELXTL package and refined with SHELXL [35]. The non-hydrogen atoms were refined with anisotropic parameters, and the hydrogen atoms were treated using a riding model and fixed isotropic thermal parameters [36]. Crystallographic data and refinement details for CPs **1** and **2** are summarized in Table 1. Selected geometric parameters for CPs **1** and **2** are presented in Table 2 and Table 3.

Table 1  
Crystal data and structure refinements for CPs **1** and **2**.

CPs	<b>1</b>	<b>2</b>
Molecular formula	$C_7H_5N_5O_3Zn$	$C_{14}H_{12}CdI_2N_8$
Formula weight	272.53	658.52
$T$ (K)	297(2)	296(2)
$\lambda$ (Å)	0.71073	0.71073
Crystal system	orthorhombic	monoclinic
Space group	$Pbca$	$P2_1/n$
$a$ (Å)	13.048(7)	4.0957(8)
$b$ (Å)	10.361(6)	30.349(6)
$c$ (Å)	13.760(8)	7.8144(15)
$\alpha$ ( $^{\circ}$ )	90	90
$\beta$ ( $^{\circ}$ )	90	94.832(3)
$\gamma$ ( $^{\circ}$ )	90	90
$V$ (Å $^3$ )	1860.2(18)	967.9(3)
$Z$	8	2
$\rho_{calc}$ (Mg/m $^3$ )	1.946	2.260
$\mu$ (mm $^{-1}$ )	2.640	4.332
$F(000)$	1088	612
Reflections collected	12307	9710
Unique reflections	1642	2799
$R_{int}$	0.1070	0.0538
Number of parameters	145	115
Goodness-of-fit (GOF)	1.076	1.232
$R_1$ [ $I > 2\sigma(I)$ ]	0.0447	0.0515
$wR_2$ [ $I > 2\sigma(I)$ ]	0.1156	0.1162
$\Delta\rho_{max}/\Delta\rho_{min}$ (e Å $^{-3}$ )	0.623/−0.710	1.064/−1.487

**Table 2**  
Selected bond lengths (Å) and angles (°) for CPs **1**<sup>a</sup> and **2**<sup>b</sup>.

[Zn(L)NO <sub>3</sub> ] <sub>n</sub> ( <b>1</b> )			
Zn(1)–N(4)#1	1.973(5)	Zn(1)–O(1)	1.985(5)
Zn(1)–N(1)	2.000(5)	Zn(1)–N(2)#2	2.009(5)
N(2)–Zn(1)#3	2.010(5)	N(4)–Zn(1)#4	1.973(5)
N(4)#1–Zn(1)–O(1)	107.7(2)	N(4)#1–Zn(1)–N(1)	116.7(2)
O(1)–Zn(1)–N(1)	112.2(2)	N(4)#1–Zn(1)–N(2)#2	115.2(2)
O(1)–Zn(1)–N(2)#2	95.7(2)	N(1)–Zn(1)–N(2)#2	107.4(2)
N(3)–N(2)–Zn(1)#3	113.1(4)	C(6)–N(2)–Zn(1)#3	135.8(4)
C(7)–N(4)–Zn(1)#4	130.0(4)	N(3)–N(4)–Zn(1)#4	120.5(4)
[Cd(L) <sub>2</sub> ] <sub>n</sub> ( <b>2</b> )			
I(1)–Cd(1)#1	2.904(6)	I(1)–Cd(1)	3.036(5)
Cd(1)–N(1)	2.373(5)	Cd(1)–N(1)#2	2.373(5)
Cd(1)–I(1)#3	2.904(6)	Cd(1)–I(1)#4	2.904(6)
Cd(1)–I(1)#2	3.037(5)	Cd(1)#1–I(1)–Cd(1)	87.1(18)
N(1)–Cd(1)–N(1)#2	180.0	N(1)–Cd(1)–I(1)#3	90.9(14)
N(1)#2–Cd(1)–I(1)#3	89.0(14)	N(1)–Cd(1)–I(1)#4	89.1(14)
N(1)#2–Cd(1)–I(1)#4	90.9(14)	I(1)#3–Cd(1)–I(1)#4	180.0(16)
N(1)–Cd(1)–I(1)#2	89.3(14)	N(1)#2–Cd(1)–I(1)#2	90.7(14)
I(1)#3–Cd(1)–I(1)#2	87.1(18)	I(1)#4–Cd(1)–I(1)#2	92.9(18)
N(1)–Cd(1)–I(1)	90.7(14)	N(1)#2–Cd(1)–I(1)	89.3(14)
I(1)#3–Cd(1)–I(1)	92.9(18)	I(1)#4–Cd(1)–I(1)	87.1(18)
I(1)#2–Cd(1)–I(1)	180.0		

Symmetry transformations used to generate equivalent atoms: <sup>a</sup>For **1**, #1x,  $-y + 5/2$ ,  $z + 1/2$ ; #2  $-x + 3/2$ ,  $-y + 2$ ,  $z + 1/2$ ; #3  $-x + 3/2$ ,  $-y + 2$ ,  $z - 1/2$ ; #4  $x$ ,  $-y + 5/2$ ,  $z - 1/2$ .

<sup>b</sup>For **2**, #1  $x + 1$ ,  $y$ ,  $z$ ; #2  $-x$ ,  $-y$ ,  $-z$ ; #3  $-x + 1$ ,  $-y$ ,  $-z$ ; #4  $x - 1$ ,  $y$ ,  $z$ .

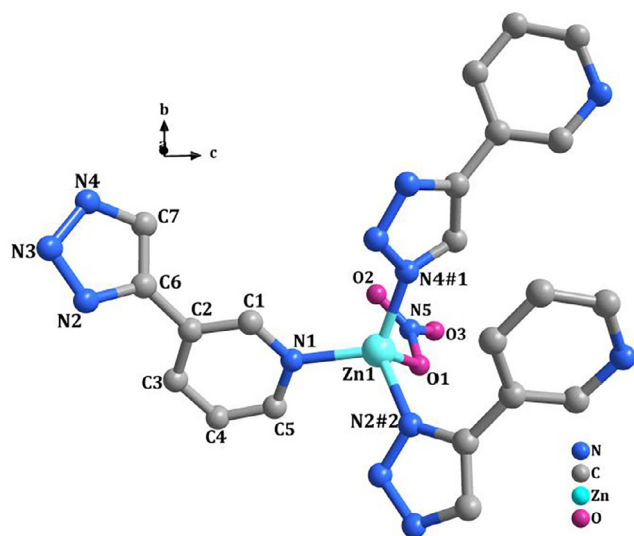


**Fig. 1.** Coordination environment of Zn(II) atoms in **1**. H atoms are omitted for clarity; Symmetry codes: #1:  $x$ ,  $-y + 5/2$ ,  $z + 1/2$ ; #2:  $-x + 3/2$ ,  $-y + 2$ ,  $z + 1/2$ .

## 2.6. Computational descriptions

The theoretical calculations were carried out using the GAUSSIAN 09 program [37]. The ground state structures were optimized and calculated by using density functional theory (DFT) at the B3LYP method with 6-311G(d) basis set for C, H, N, O and LanL2DZ basis set for Zn, Cd and I [38–42]. The geometries optimization at the first singlet excited state were carried out at the same level using the time-dependent density functional theory (TD-DFT). Convergence criteria are program defaults. In order to simulate the absorption and emission processes, the vertical excitations of singlet states at the B3LYP level were calculated by TD-DFT method at the optimized geometries in the ground and excited states. The base set is the same as above. Molecular orbitals cube files were generated and visualized with GaussView [43,44]. The hydrogen

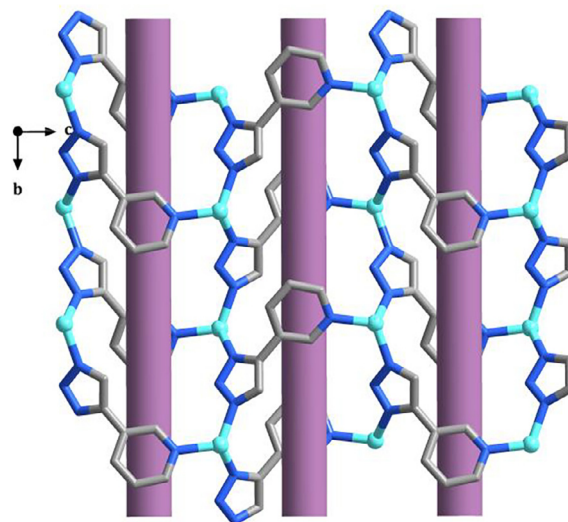


**Fig. 2.** The 2D sheet structure of **1**. H atoms and NO<sub>3</sub><sup>−</sup> anions are omitted for clarity.

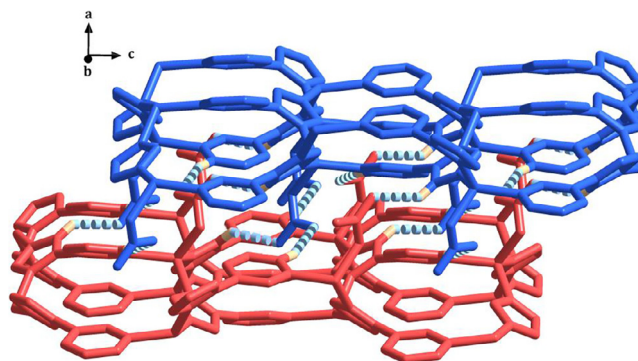


**Fig. 3.** Perspective view of the hydrogen-bonded (pale blue dashed lines) 3D supramolecular network of **1**. Symmetry codes: #6:  $-x + 2$ ,  $y - 1/2$ ,  $-z + 1/2$ ; #7:  $-x + 2$ ,  $y + 1/2$ ,  $-z + 1/2$ . (Color online.)

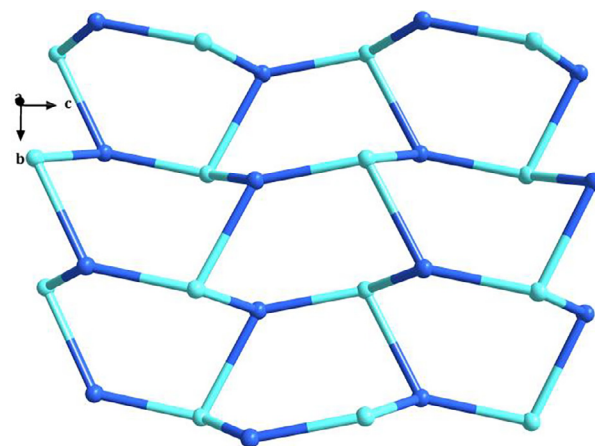


**Fig. 4.** The (3,3)-connected net topology with the point symbol of (6<sup>3</sup>) (turquoise balls: 3-connected ligand node, light blue balls: 3-connected metal node). (Color online.)

bond interaction energies were calculated with DFT using the ωB97XD functional and 6-311G(d) basis set. Basis-set superposition error (BSSE) was corrected by counterpoise method [45]. The



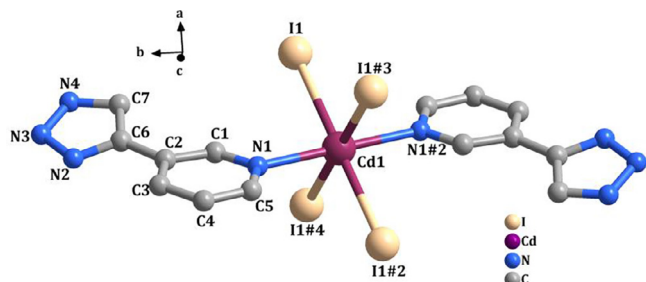


**Fig. 5.** Coordination environment of Cd(II) atoms in **2**. H atoms are omitted for clarity; Symmetry codes: #1:  $x+1, y, z$ ; #2:  $2-x, -y, -z$ ; #3:  $-x+1, -y, -z$ ; #4:  $x-1, y, z$ .

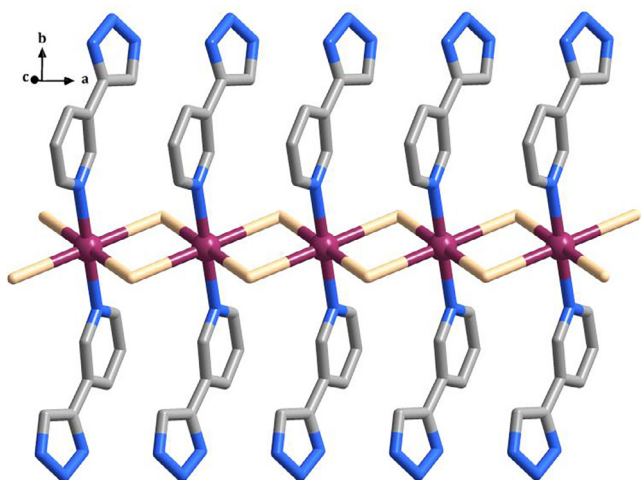


**Fig. 6.** View of the 1D chain structure of **2**.

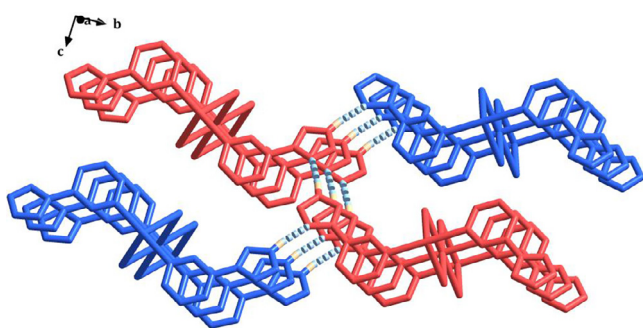


**Fig. 7.** Perspective view of the 3D supramolecular network built from 1D inorganic-organic infinite chain via hydrogen bonds in **2** (pale blue dashed lines). Symmetry codes: #5:  $x+1/2, -y+1/2, z-1/2$ . (Color online.)

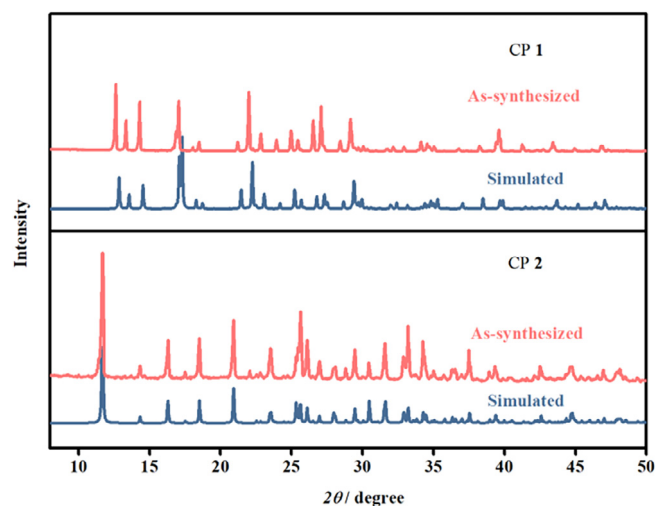
intermolecular HOMO-HOMO and LUMO-LUMO overlap integrals were calculated accurately by using Multiwfn 3.6 program [46].

### 3. Results and discussion

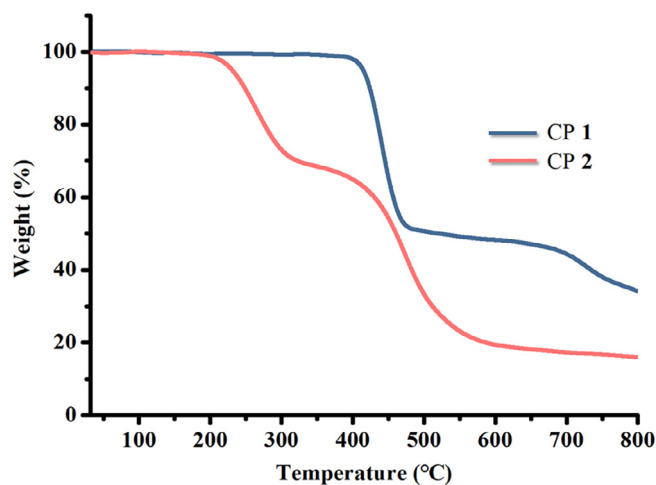
#### 3.1. Description of crystal structure

##### 3.1.1. Structure of $[Zn(L)NO_3]_n$ (**1**)

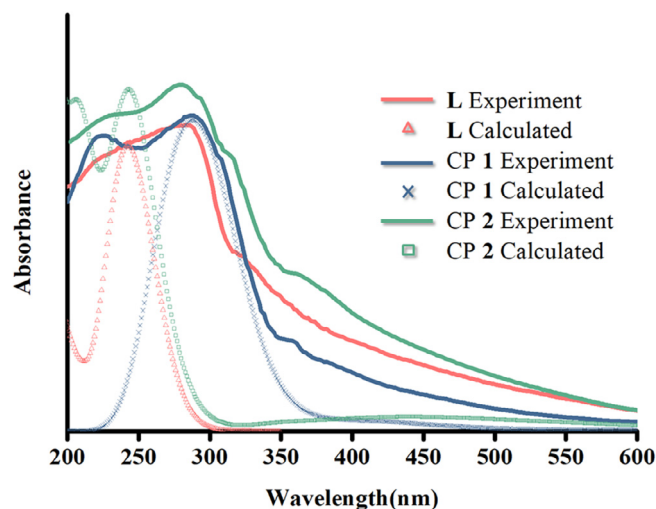
X-ray diffraction analyses reveals that complexes **1** crystallizes in the orthorhombic system with space group  $Pbca$ . The asymmetric unit composed of one Zn(II) ion, one bridging **L** ligand and one



**Fig. 8.** XRD patterns of CPs **1–2** (blue: simulated from X-ray single crystal data, red: as-synthesized sample). (Color online.)



**Fig. 9.** TGA curves for CPs **1** and **2**.

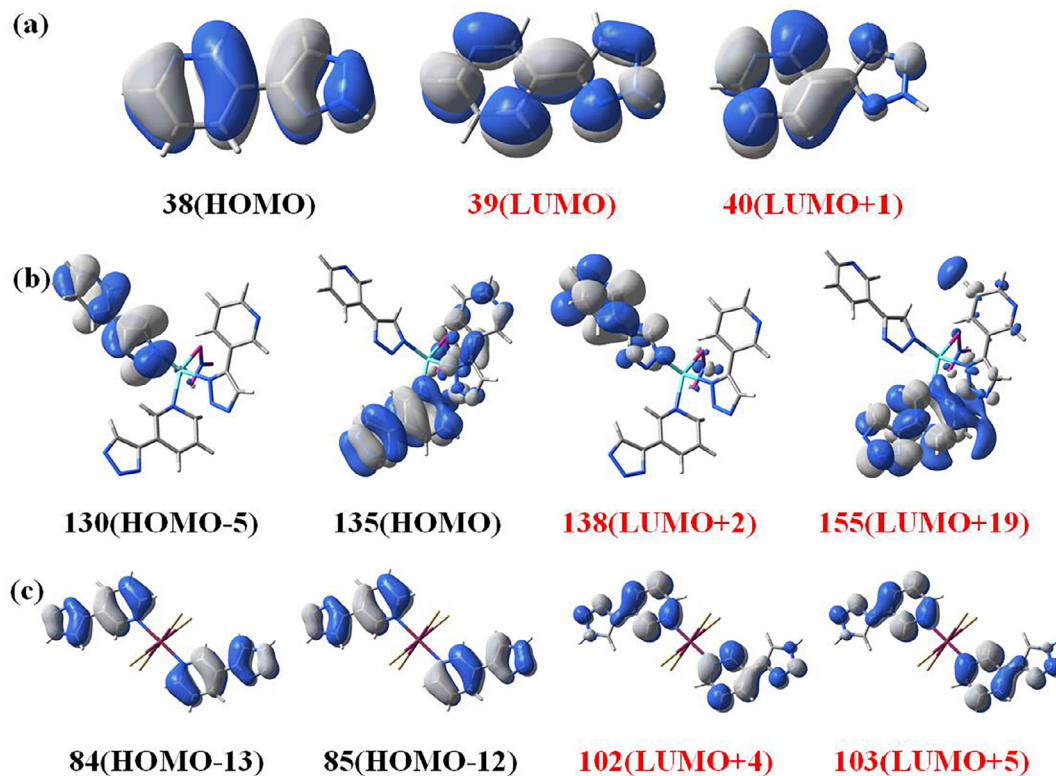
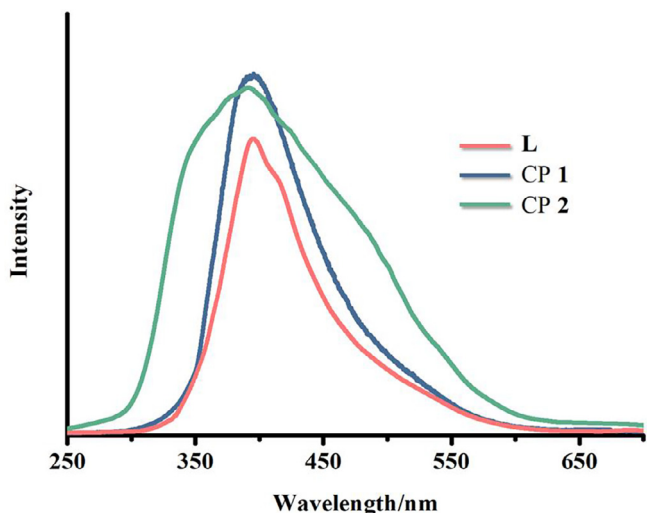


**Fig. 10.** Absorption spectra of **L**, CPs **1** and **2** obtained from experiment and TD-DFT calculation.

**Table 3**Hydrogen bonding geometry for CPs **1**<sup>c</sup> and **2**<sup>d</sup>.

D–H...A	d(D–H)/Å	d(H...A)/Å	d(D...A)/Å	∠D–H...A/(°)
<i>[Zn(L)NO<sub>3</sub>]<sub>n</sub></i> ( <b>1</b> )				
C(4)–H(4)...O(1)#5	0.93	2.45	3.301(8)	151.4
C(5)–H(5)...O(2)#6	0.93	2.61	3.483(9)	157.4
C(7)–H(7)...O(3)#7	0.93	2.46	3.216(9)	138.8
<i>[Cd(L)I<sub>2</sub>]<sub>n</sub></i> ( <b>2</b> )				
N(4)–H(4)...N(2)#5	0.861(6)	1.935(5)	2.789(8)	171.2(5)

Symmetry transformations used to generate equivalent atoms: <sup>c</sup>For **1**, #5x, –y + 3/2, z – 1/2; #6 –x + 2, y – 1/2, –z + 1/2; #7 –x + 2, y + 1/2, –z + 1/2. <sup>d</sup>For **2**, #5: x + 1/2, –y + 1/2, z – 1/2.

**Fig. 11.** Molecular orbitals related to the main transitions for **L** (a), CPs **1** (b) and **2** (c).**Fig. 12.** The solid fluorescence emission spectra of ligand, CPs **1** and **2** at 298 K.

NO<sub>3</sub><sup>-</sup> anion. As shown in Fig. 1, the central Zn(II) ion is four-coordinated in an approximately tetrahedral coordination environment, which is defined by four nitrogen atoms originating from three independent **L** ligands and one oxygen atom (O1) of the NO<sub>3</sub><sup>-</sup> with the coordination angles around zinc centre varying from 95.7(2)° to 116.7(2)°. The Zn–O bond (1.985(5) Å), and Zn–N (2.000(5) Å, 2.009(5) Å and 1.973(5) Å) are comparable to some analogs [47]. These Zn(II) ions are bridged by  $\mu_3$ -**L** nitrogen atoms (N1, N2 and N4) to form a **hcb** coordination 2D layer in the *ab* plane (Fig. 2). **L** ligands and three Zn(II) ions form a 19-membered ring. Furthermore, the 2D layer is interconnected via two types of hydrogen bonds (C(5)...O(2)#6 (3.483(9) Å, 157.4°) and C(7)...O(3)#7 (3.216(9) Å, 138.8°) to result in a 3D supramolecular framework (Fig. 3). For a better understanding of the intricate framework, a topological analysis of complex **1** was performed. In the 2D layer, the Zn(II) ions and **L** ligands can be defined as three-connected nodes, respectively. Thus, the network topology of **1** can be simplified as a binodal (3,3)-connected layer with the point symbol of (6<sup>3</sup>) (Fig. 4).

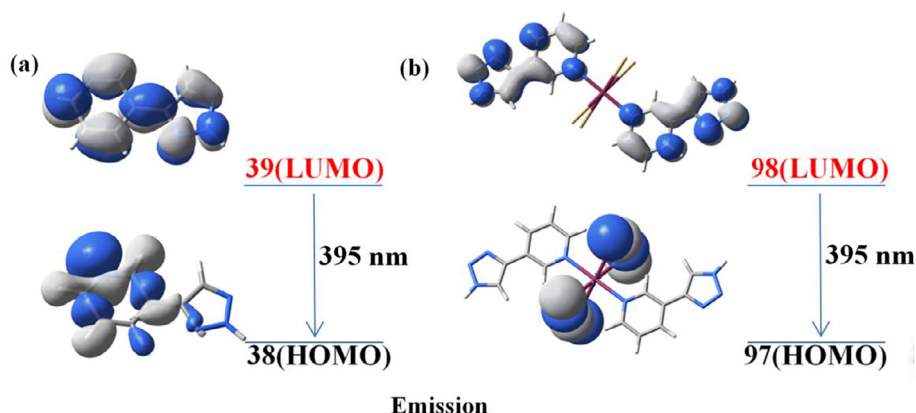


Fig. 13. Main calculated electronic transitions contributing to the emission processes for **L** (a) and **CP 2** (b).

Table 4

Properties of selected transitions and their contributions of **L**, **CPs 1** and **2**.

	Excited State	Transition energy (eV)	Wavelength (nm)	Oscillator <i>f</i>	Contributions
<b>L</b>	2	4.8851	253.80	0.1746	38–39 (67.82%)
	4	5.2418	236.53	0.2491	38–40 (52.69%)
<b>CP 1</b>	43	4.0481	306.28	0.4416	135–155 (48.64%)
	51	4.3966	282.00	0.3833	130–138 (56.52%)
<b>CP 2</b>	139	5.2584	235.78	0.4148	84–102 (33.43%)
					85–103 (32.17%)

### 3.1.2. Structure of $[\text{Cd}(\text{L})\text{I}_2]_n$ (**2**)

X-ray crystallographic analyses reveals that complexes **2** crystallizes in the monoclinic system with space group  $P2_1/n$ . The asymmetric unit composed of one Cd(II) ion, one bridging **L** ligand and one  $\text{I}^-$  anion. The Cd1 ion is six coordinated with an octahedral coordination geometry, which is fulfilled by four iodine anions and two nitrogen atoms originating from two independent **L** ligands with the coordination angles varying from  $87.1(18)^\circ$  to  $180.0(16)^\circ$ . The Cd–N bond length is  $2.373(5)$  Å, and the lengths of Cd–I bonds are  $3.037(5)$  Å,  $2.904(6)$  Å, respectively. The four iodine anions are located in the equatorial plane and the two nitrogen atoms are located at the axial position of the octahedron (Fig. 5). The octahedron  $[\text{Cd}(1)\text{N}_2\text{I}_4]$  is edged-shared with two iodine anions (I1, I1#3) to form a 4-membered ring  $[\text{Cd}_2(1)\text{I}_2]$ . The two equivalent Cd(II) atoms are interconnected via two  $\mu_2$ -I bridges to give an infinite 1D chain along the *a*-axis with the Cd...Cd distance of  $4.096(8)$  Å (Fig. 6). Next, the 1D chains are stacked together in the *bc* plane, producing a three-dimensional supramolecular network (Fig. 7) through hydrogen bonds which exist in the nitrogen atom N(4) and the nitrogen atom N(2)#5 from the triazoles of two different ligands as follow:  $\text{N4}\cdots\text{N2\#5}$  ( $2.789(8)$  Å,  $171.2^\circ$ ).

### 3.2. Powder X-ray diffraction and thermogravimetric analysis

The as-synthesized products of **CPs 1** and **2** were characterized by X-ray powder diffraction (XRD). As shown in Fig. 8, the measured powder XRD patterns closely match the results simulated from single crystal data, thus indicating the high phase purity of as-synthesized samples.

To investigate the thermal stabilities of **CPs 1** and **2**, thermogravimetric analyses (TGA) were carried out (Fig. 9) from  $30$  to  $800^\circ\text{C}$  under a nitrogen atmosphere with a heating rate of  $10^\circ\text{C}/\text{min}$ . The TGA curves indicate that cyclic **CPs 1** and **2** are thermally stable to  $420$  and  $220^\circ\text{C}$ , respectively. For **CP 1**, a weight loss is observed in the temperature range  $420$ – $500^\circ\text{C}$ , reflecting the loss of 4-(3-Pyridyl)-2H-1,2,3-triazole ligand (51.51%, calculated value 53.23%). For **CP 2**, the TGA curve presents two main stages of

decomposition. There is weight loss of approximately 35.11% from  $220$  to  $310^\circ\text{C}$ , corresponding to the loss of  $\text{I}^-$  anion (38.54% calcd). And a second weight loss of approximately 45.23% (calculated value 44.34%) from  $400$  to  $600^\circ\text{C}$ , which can be attributed to the removal of the organic ligand (calculated value 44.34%).

### 3.3. Optical properties

#### 3.3.1. Absorption spectra

UV–Vis absorption spectra of ligand **L**, **CPs 1** and **2** in the  $\text{BaSO}_4$  plate and theoretical absorption spectra have been measured and calculated, respectively. As displayed in Fig. 10, the absorption spectra of **L**, **CPs 1** and **2** obtained from the TD-DFT calculations are in qualitative agreement with the experimental observations. Apparently, the ligand **L**, **1** and **2** display similar absorption spectra, where the characteristic band centered at  $280$  nm in the high-

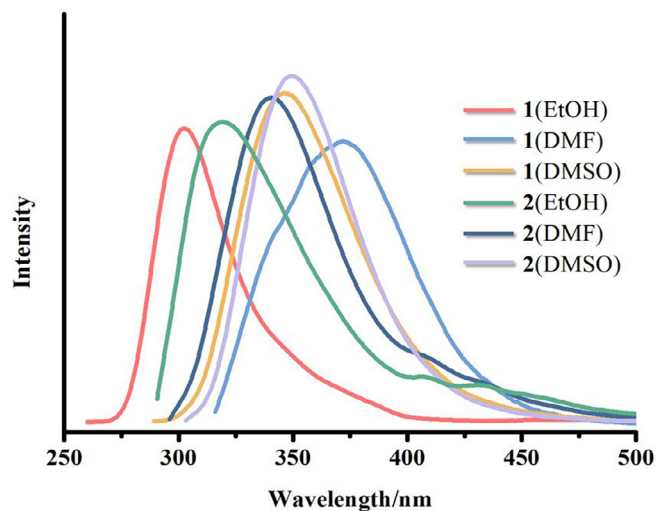
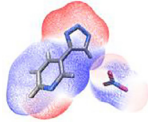
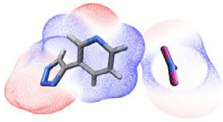
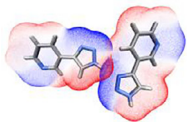


Fig. 14. The emission spectra of **CPs 1** and **2** in different solvents.

**Table 5**Properties of selected transitions and their contributions to the emission processes for **L** and CP **2**.

	Excited State	Transition energy (eV)	Wavelength (nm)	Oscillator $f$	Contributions
<b>L</b>	1	3.3481	370.31	0.0023	38–39 (97.41%)
CP <b>2</b>	1	3.0994	400.03	0.0017	97–98 (97.84%)

**Table 6**The calculated hydrogen bonding interaction energies of **1** and **2**.

Type	C(7)–H(7)···O(3)#7	C(5)–H(5)···O(2)#6	N(4)–H(4)···N(2)#5
Electrostatic Potential Map			
HOMO–HOMO	0.00764952	0.00777467	0.00051007
LUMO–LUMO	0.00024445	–0.00044539	–0.00073905
E(AB)/a.u.	–768.6564546	–768.6538703	–978.2495612
E(A)/a.u.	–488.445386615	–488.445410535	–489.1164802
E(B)/a.u.	–280.197409998	–280.197429946	–489.1164725
E(BSSE)/a.u.	0.001697079864	0.001102290628	0.00212628
E(interaction)/a.u.	–0.011960887	–0.009927559	–0.014482232

energy side, no considerable absorption in the visible spectroscopy region.

The calculated data are collected in Table 4 and the molecular orbitals (MOs) are shown in Fig. 11. The MOs of **L** ligand related to the main transitions are illustrated in Fig. 11a. The absorption band (at ~280 nm) of **L** is mainly attributed to the transition of states 2 and 4. The transitions of states 2 and 4 include the orbitals 38–39 (67.82%) and 38–40 (52.69%), respectively, which reveals a partial contribution originating from conjugated systems of pyridine and triazole groups. As shown in Fig. 11b, the absorption band for CP **1** at ~280 nm should be ascribed to states 43 and 51. The transitions of the states 43 and 51 contain orbitals 135–155 (48.64%) and 130–138 (56.52%), which is mainly attributed to the  $\pi$ – $\pi^*$  transition of the **L** ligand and the interligand charge transfer. By analysis of MOs of CP **2** involved with the main transitions (Fig. 11c), the calculated results show that the absorption process (at ~280 nm) is due to the electronic transition from state 139. For state 139, the transitions containing orbitals 84–102 (33.43%) and 85–103 (32.17%) are assigned to  $\pi$ – $\pi^*$  transitions of the pyridine and triazole groups.

### 3.3.2. Fluorescent properties

The solid-state emission spectra for free ligand, CPs **1** and **2** were investigated at 298 K (Fig. 12). They display same maximum emission of 395 nm under the 334 nm excitation wavelength. To further understand the emission properties of **L** and CP **2**, theoretical calculations are carried out using density functional theory (DFT) with B3LYP functional. The main electronic transitions that contribute to the emission processes are illustrated in Fig. 13, and the properties of selected transitions and their contributions to the emission processes are collected in Table 5. **L** and CP **2** have similar emission processes and give almost the same electronic density involved from the lowest unoccupied molecular orbital (LUMO) to highest occupied molecular orbital (HOMO) [47]. The electronic transitions in the emission processes are attributed to the  $\pi^* \rightarrow n$  transitions of the **L** ligand and the **L** ligand to iodine ion (Fig. 13).

Further, the fluorescence properties of CPs **1** and **2** have been investigated at 298 K in different solvents such as dimethyl sulfoxide (DMSO), ethanol (EtOH) and N, N-dimethylformamide (DMF) (Fig. 14). For CP **1**, the emissions differ in different solvents

and range from 302 to 372 nm. **1** in DMF, DMSO and EtOH solutions exhibit blue luminescences with  $\lambda_{\text{max}} = 372$ , 345 and 302 nm, respectively. Similar to CP **1**, the solutions luminescences of CP **2** all produce blue luminescences at 318–350 nm by using DMF, DMSO and EtOH as the coordinating solvents. The above solvents play different roles with photoactive metal centers in the solution state. For CPs **1** and **2**, the emission band of their solutions are all showing an obvious blue-shift compared with their luminescence at solid state, which can be ascribed as the increase of the excited-state energy caused by the solvent molecules [26].

### 3.4. Hydrogen bond interaction energy

In order to better understand the energetic feature of the supramolecular interactions in CPs **1** and **2**, the hydrogen bond interaction energies were calculated using DFT  $\omega$ B97XD, 6-311G (d) basis set. Basis-set superposition error (BSSE) was corrected by counterpoise method [45]. Intermolecular weak interaction energy can be defined as:

$$E_{\text{(interaction)}} = E_{\text{(AB)}} - E_{\text{(A)}} - E_{\text{(B)}} + E_{\text{(BSSE)}}$$

$E_{\text{(AB)}}$  is the energy of dimer AB,  $E_{\text{(A)}}$  is the energy of monomer A under A basis group,  $E_{\text{(B)}}$  is the energy of monomer B under B basis group.  $E_{\text{(BSSE)}}$  is the energy of basis-set superposition error (BSSE).

The hydrogen bond energies, the electrostatic potential maps and the overlap integrals of HOMO–HOMO and LUMO–LUMO of CPs **1** and **2** are listed in Table 6. The energies of two hydrogen bonds in CP **1** are 31.40 and 26.06 kJ/mol, and 38.02 kJ/mol in CP **2**. It can be judged from the energy and distance of hydrogen bond that the interaction is weak in strength. In the electrostatic potential maps, red represents regions of most positive electrostatic potential, blue represents regions of most negative electrostatic potential, and white represents region of zero potential. Potential increases in the order blue < white < red. The positive value of overlap integral indicates that the degree of same phase overlap between HOMO–HOMO or LUMO–LUMO is greater than that of the opposite way, and the overlap is mainly in the same phase. But the overlap integral is negative, which indicates that the opposite phase overlap is greater, and the overlap is mainly in the opposite phase.



## 4. Conclusion

Two  $d^{10}$  transition metal CPs,  $[\text{Zn}(\text{L})\text{NO}_3]_n$  (**1**) and  $[\text{Cd}(\text{L})_2]_n$  (**2**), have been successfully constructed and characterized based on the new ligand of 4-(3-Pyridyl)-2H-1,2,3-triazole. CP **1** reveals a **hcb** (3,3)-connected 2D framework and further forms a supramolecular 3D structure via H-bonding interactions. CP **2** displays a 1D straight chain and hydrogen bonding leads to the formation of supramolecular 3D system. The TD-DFT calculation is performed on ligand **L**, CPs **1** and **2** and further confirmed by the results of experimental UV–Vis spectra, which fit well to the calculated ones. The results of calculations confirm that the absorption processes mainly origin as  $\pi-\pi^*$  charge transition. The fluorescence emission spectra reveal all the compounds have unique fluorescent emissions in different solvents and solid-state.

## Acknowledgments

The authors thank the financial support from the National Natural Science Foundation of China (No. 21301132, 51402221, 51472186, 51372177) and the Scholarship Foundation of China Scholarship Council (201708420019).

## Appendix A. Supplementary data

CCDC 1878721 and 1878722 contains the supplementary crystallographic data for CPs **1** and **2**. These data can be obtained free of charge via <http://www.ccdc.cam.ac.uk/conts/retrieving.html>, or from the Cambridge Crystallographic Data Centre, 12 Union Road, Cambridge CB2 1EZ, UK; fax: (+44) 1223-336-033; or e-mail: [deposit@ccdc.cam.ac.uk](mailto:deposit@ccdc.cam.ac.uk).

## References

- [1] S. Noro, J. Mizutani, Y. Hijikata, R. Matsuda, H. Sato, S. Kitagawa, K. Sugimoto, Y. Inubushi, K. Kubo, T. Nakamura, Nat. Commun. 6 (2015) 5851.
- [2] J.S. Qin, D.Y. Du, M. Li, X.Z. Lian, L.Z. Dong, M. Bosch, Z.M. Su, Q. Zhang, S.L. Li, Y. Q. Lan, J. Am. Chem. Soc. 138 (2016) 5299.
- [3] J.-R. Li, J. Sculley, H.-C. Zhou, Chem. Rev. 112 (2012) 869.
- [4] M. Yoon, R. Srirambalaji, K. Kim, Chem. Rev. 112 (2012) 1196.
- [5] D. Yang, W. Xu, X. Cao, S. Zheng, J. He, Q. Ju, Z. Fang, W. Huang, Inorg. Chem. 55 (2016) 7954.
- [6] Y. Li, Y. Hu, Y. Zhao, G. Shi, L. Deng, Y. Hou, L. Qu, Adv. Mater. 23 (2011) 776.
- [7] Y.L. Chang, O.K. Farha, B.J. Hong, A.A. Sarjeant, S.B.T. Nguyen, J.T. Hupp, J. Am. Chem. Soc. 133 (2011) 15858.
- [8] C.A. Kent, B.P. Mehl, L. Ma, J.M. Papanikolas, T.J. Meyer, W. Lin, J. Am. Chem. Soc. 132 (2010) 12767.
- [9] W. Shi, H. Fan, S. Ai, L. Zhu, New J. Chem. 39 (2015) 7054.
- [10] T. Wen, B. Yang, Y. Guo, J. Sun, C. Zhao, S. Zhang, M. Zhang, Y. Wang, Phys. Chem. Chem. Phys. 16 (2014) 23188.
- [11] K. Biradha, C. Seward, M.J. Zaworotko, Helical Coordination Polymers with Large Chiral Cavities, Angew. Chem., Int. Ed. 38 (4) (1999) 492.
- [12] O. Evans, R. Xiong, Z. Wang, et al., Crystal Engineering of acentric diamondoid metal-organic coordination networks, Angew. Chem. Int. Ed. 38 (4) (2010) 536.
- [13] T.K. Prasad, M.V. Rajasekharan, J.P. Costes, A cubic 3d–4f structure with only ferromagnetic Gd–Mn interactions, Angew. Chem., Int. Ed. 46 (16) (2007) 2851.
- [14] Q. Li, D.-X. Xue, Y.-F. Zhang, Z.-H. Zhang, Z. Gao, J. Bai, J. Mater. Chem. A 5 (2017) 14182.
- [15] J. Lee, Y. Kang, N.S. Cho, K.-M. Park, Cryst. Growth Des. 16 (2016) 996.
- [16] B. Ay, E. Yildiz, I. Kani, Polyhedron 142 (2018) 1.
- [17] F. Grifasi, M.R. Chierotti, C. Garino, R. Gobetto, E. Priola, E. Diana, F. Turci, Cryst. Growth Des. 15 (2015) 2929.
- [18] K. Li, L.-M. Zhu, L.-L. Qian, Z.-X. Wang, B.-L. Li, H.-Y. Li, Polyhedron 145 (2018) 53.
- [19] H. Huang, M. Beuchel, Y. Park, P.J. Baesjou, S.C.J. Meskers, D.M. de Leeuw, K. Asadi, J. Phys. Chem. C 120 (2016) 11045.
- [20] X. Song, X. Zhou, W. Liu, W. Dou, J. Ma, X. Tang, J. Zheng, Inorg. Chem. 47 (2008) 11501.
- [21] D.M. Zink, T. Baumann, J. Friedrichs, M. Nieger, S. Bräse, Inorg. Chem. 52 (2013) 13509.
- [22] C. Baik, W.S. Han, Y. Kang, S.O. Kang, J. Ko, J. Organomet. Chem. 691 (2006) 5900.
- [23] Y. Cui, H. Xu, Y. Yue, Z. Guo, J. Yu, Z. Chen, J. Gao, Y. Yang, G. Qian, B. Chen, J. Am. Chem. Soc. 134 (2012) 3979.
- [24] L. Zhai, Z.X. Yang, W.W. Zhang, J.L. Zuo, X.M. Ren, Inorg. Chem. 57 (2018) 4171.
- [25] C. Yue, F. Jiang, Y. Xu, D. Yuan, L. Chen, C. Yan, M. Hong, Cryst. Growth Des. 8 (2008) 2721.
- [26] C.-H. Jiang, Y.-M. Qi, Y. Sun, Q. Chi, Y.-M. Guo, J. Mol. Struct. 1017 (2012) 65.
- [27] T.U. Connell, C. Schieber, L.P. Silvestri, J.M. White, S.J. Williams, P.S. Donnelly, Inorg. Chem. 53 (2014) 6503.
- [28] A. Mandal, B.K. Patel, Polyhedron 132 (2017) 112.
- [29] J.-X. Chen, K. Wang, C.-J. Zheng, M. Zhang, Y.-Z. Shi, S.-L. Tao, H. Lin, W. Liu, W.-W. Tao, X.-M. Ou, X.-H. Zhang, Adv. Sci. 5 (2018) 1800436.
- [30] V.K. Outlaw, J. Zhou, A.E. Bragg, C.A. Townsend, RSC Adv. 6 (2016) 61249.
- [31] L.-H. Cao, Y.-L. Wei, Y. Yang, H. Xu, S.-Q. Zang, H.-W. Hou, T.C.W. Mak, Cryst. Growth Des. 14 (2014) 1827.
- [32] S. Sen, T. Yamada, H. Kitagawa, P.K. Bharadwaj, Cryst. Growth Des. 14 (2014) 1240.
- [33] K. Xing, R. Fan, S. Gao, X. Wang, X. Du, P. Wang, R. Fang, Y. Yang, Dalton Trans. 45 (2016) 4863.
- [34] Q. Hu, Y. Liu, X. Deng, Y. Li, Y. Chen, Adv. Synth. Catal. 358 (2016) 1689.
- [35] G. Sheldrick, Acta Crystallogr. Sect. A 64 (2008) 112.
- [36] G. Sheldrick, Acta Crystallogr. Sect. C 71 (2015) 3.
- [37] M. J. Frisch, G. W. Trucks, H. B. Schlegel, et al., Gaussian, Inc., Wallingford CT, 2016.
- [38] D. Majumdar, M.S.S. Babu, S. Das, J.K. Biswas, M. Mondal, S. Hazra, J. Mol. Struct. 1138 (2017) 161.
- [39] T.R. And, W.L. Jorgensen, J. Chem. Theory Comput. 4 (2008) 297.
- [40] I.F.A. Mariz, E.M.S. Macôas, J.M.G. Martinho, L. Zou, P. Zhou, X. Chen, J. Qin, J. Mater. Chem. B 1 (2013) 2169.
- [41] A.H. Chen, S.C. Meng, K. Zhou, C.C. Wang, W. Zhao, A.J. Wang, J. Qian, J. Chem. Sci. 129 (2017) 1.
- [42] C. Sen, A. Nandi, D. Mallick, S. Mondal, K.K. Sarker, C. Sinha, Spectrochim. Acta Part A Mol. Biomol. Spectrosc. 137 (2015) 935.
- [43] W.T. Gong, X.M. Qian, F.R. Wang, Y. Lin, G.L. Ning, Heteroat. Chem. 24 (2013) 66.
- [44] B. Holló, Z.D. Tomić, P. Pogány, A. Kovács, V.M. Leovac, K.M. Szécsényi, Polyhedron 28 (2009) 3881.
- [45] S.F. Boys, F. Bernardi, Mol. Phys. 19 (1970) 553.
- [46] Lu. Tian, Feiwu Chen, J. Comput. Chem. 33 (2012) 580.
- [47] L.E.I. Xue, C.H.E.N. Yun-Zhou, L.I. Yuan-Xiang, J.I.A. Li-Hui, C.H.E.N. Yun-Feng, Chin. J. Inorg. Chem. 34 (2018) 545.